






Spatially inhomogeneous superconductivity in UTe_2 S. M. Thomas ¹, C. Stevens ², F. B. Santos ³, S. S. Fender ¹, E. D. Bauer,¹ F. Ronning ¹, J. D. Thompson,¹
A. Huxley,² and P. F. S. Rosa¹¹*Los Alamos National Laboratory, Los Alamos, New Mexico 87545, USA*²*School of Physics and Astronomy, University of Edinburgh, Edinburgh EH9 3FD, United Kingdom*³*Escola de Engenharia de Lorena, Universidade de Sao Paulo (EEL-USP),
Materials Engineering Department (Demar), Lorena, Sao Paulo 12602-810, Brazil*

(Received 10 September 2021; revised 16 November 2021; accepted 17 November 2021; published 3 December 2021)

The newly discovered superconductor UTe_2 is a strong contender for a topological spin-triplet state wherein a multicomponent order parameter arises from two nearly degenerate superconducting states. A key issue is whether both of these states intrinsically exist at ambient pressure. Through thermal expansion and calorimetry, we show that UTe_2 at ambient conditions exhibits two detectable transitions only in some samples, and the size of the thermal expansion jump at each transition varies when the measurement is performed in different regions of the sample. This result indicates that the two transitions arise from two spatially separated regions that are inhomogeneously mixed throughout the volume of the sample, each with a discrete superconducting transition temperature (T_c). Notably, samples with higher T_c only show a single transition at ambient pressure. Above 0.3 GPa, however, two transitions are invariably observed in ac calorimetry. Our results not only point to a nearly vertical line (constant pressure) in the pressure-temperature phase diagram but also provide a consistent scenario for the sample dependence of UTe_2 .

DOI: [10.1103/PhysRevB.104.224501](https://doi.org/10.1103/PhysRevB.104.224501)

I. INTRODUCTION

UTe_2 is a recently discovered superconductor that exhibits many intriguing properties. Even though UTe_2 does not exhibit long-range magnetic order above 25 mK, initial reports placed UTe_2 as a new example of a spin-triplet superconductor due to an upper critical field (H_{c2}) exceeding 30 T and scaling of the magnetization indicating proximity to a ferromagnetic quantum critical point [1–3]. Importantly, superconductivity in UTe_2 may be topological. Asymmetric tunneling was observed across step edges in scanning tunneling microscopy, consistent with chiral superconductivity [4]. Polar Kerr effect measurements combined with theoretical modeling revealed that the superconducting order parameter breaks time-reversal symmetry and is likely to contain Weyl nodes [5]. More recently, magnetic penetration depth measurements revealed temperature scaling consistent with a multicomponent spin-triplet state [6].

UTe_2 also exhibits striking phase diagrams as a function of applied pressure and magnetic fields. For instance, reentrant superconductivity is observed for fields applied in the orthorhombic bc plane, whereas a metamagnetic transition occurs near 30 T for fields parallel to the b axis [7–9]. Under pressure, UTe_2 remains equally puzzling, and a complete agreement between the many reports has yet to be reached. One common aspect is the existence of multiple superconducting transitions under pressures above about 0.3 GPa [10–14]. One superconducting transition (T_{c1}) reaches a maximum of about 3 K at a pressure near 1.2 GPa, and a second superconducting transition (T_{c2}) is suppressed monotonically with pressure. Above 1.2 GPa, T_{c1} is rapidly

suppressed and a new nonsuperconducting ordered phase emerges. Though this phase was initially thought to be the ferromagnetic state responsible for fluctuations leading to spin-triplet superconductivity at zero pressure, more recent reports argue for antiferromagnetic order under pressure due to the presence of two magnetic phase transitions as a function of temperature and their suppression as a function of all applied field directions [13,14]. Magnetic susceptibility and magnetization measurements under pressure provided further support for antiferromagnetic order above 1.2 GPa [15]. Neutron measurements found that inelastic scattering is dominated by incommensurate spin fluctuations [16,17] in spite of muon spin resonance and nuclear magnetic resonance experiments arguing for ferromagnetic fluctuations [3,18]. It was later argued that antiferromagnetic fluctuations may be responsible for superconductivity in UTe_2 [19].

A key point of contention is the low-pressure region of the phase diagram. Whether two superconducting transitions exist at ambient pressure or inhomogeneities drive a split transition remains an open question. On one hand, two nearby transitions were observed in heat capacity by Hayes *et al.*, and the Kerr effect sets in only at temperatures below the lower-temperature transition [5]. On the other hand, a composition dependence study argued that the highest-quality samples only show a single transition in heat capacity [20]. A two-component order parameter, however, is necessary for the proposed Weyl superconductivity and nonzero Kerr effect. Because of the orthorhombic structure of UTe_2 , there is no underlying symmetry argument for the existence of a two-component order parameter, and the existence of two nearby transitions would therefore be accidental.

Here, we report thermal expansion, magnetostriction, and heat capacity measurements on a number of UTe_2 samples obtained from separate growths to show that growth conditions may lead to two discrete transitions arising from an unusual form of sample inhomogeneity. In this case, we find clear evidence for two nearby transitions in the heat capacity measurements, which are accompanied by jumps in the thermal expansion coefficient. The relative size of these jumps varies as the measurement is performed on different volumes of the sample, either via thermal expansion or calorimetry measurements. Importantly, samples with higher T_c only show a single transition at ambient pressure, but all samples measured under applied pressure show at least two detectable superconducting transitions above a threshold pressure. In samples that show multiple transitions at ambient pressure, a reevaluation of the initial pressure work found that the two transitions at ambient pressure have the same pressure dependence (see the erratum to Ref. [14]).

Though we cannot unambiguously rule out the possibility of a multicomponent order parameter at ambient pressure for samples with higher T_c , our results show no evidence for a second thermodynamic transition below 0.3 GPa. Because all irreducible representations in UTe_2 are one dimensional, any transition to a multicomponent superconducting state should occur as two separate transitions as a function of temperature [5]. Even if the two transitions are perfectly degenerate at ambient pressure, they should not have the same pressure dependence because they come from independent representations. Thus, there are only two unlikely possibilities for a multicomponent order parameter in UTe_2 at zero pressure: (1) Both the transition temperature and hydrostatic pressure dependence of the two transitions are accidentally degenerate, or (2) the lower-temperature transition has immeasurably low entropy up to the crossing point of 0.3 GPa at which point it can be observed in thermodynamic measurements. Such unlikely scenarios require exceptional fine tuning. A more likely possibility is that of a nearly vertical line (constant pressure) in the pressure-temperature phase diagram. One final possibility is that some unknown mechanism keeps the two transitions pinned to the same temperature up to 0.3 GPa, which would require the formulation of a microscopic model going beyond Ginzburg-Landau arguments.

Samples of UTe_2 were grown using the vapor transport method [1,20]. About 20 batches were grown, and representative samples from many different batches were used in this study. Samples grown at higher temperatures (i.e., 1060–1000 °C gradient, sample 2) were more likely to show a split transition than samples grown at lower temperatures (e.g., 950–860 °C gradient, sample 1). Heat capacity measurements were performed down to ^3He temperatures using the quasiadiabatic relaxation technique. Thermal expansion and magnetostriction measurements were performed using a capacitance dilatometer described in Ref. [21] in both ^4He and adiabatic demagnetization cryostats. All thermal expansion measurements were performed using a slow continuous temperature ramp, whereas all magnetostriction measurements were performed by stabilizing the field to avoid the influence of eddy currents. Thermal expansion data were corrected by performing a background subtraction of the cell effect under identical thermal conditions. The ac calorimetry measure-

ments [22] were performed in a piston clamp pressure cell. Samples with the same number (1A/1B and 2A/2B) came from the same batch and showed similar zero-pressure heat capacity data. Samples were aligned for thermal expansion measurements using a Laue diffractometer.

II. RESULTS

Figure 1 shows a comparison of thermal expansion and heat capacity between three samples grown under different conditions (for additional samples see Supplemental Fig. S1 [23]). Samples 5 and 1A show a single transition at $T_c = 1.84$ K and $T_c = 1.76$ K, respectively. Sample 2A shows two transitions at $T_{c2} = 1.67$ K and $T_{c1} = 1.46$ K. The difference between these samples highlights the key role of growth conditions on the ambient pressure properties of UTe_2 .

Importantly, even samples with similar T_c may have different properties. For instance, samples 5 and 1A have similar heat capacity behavior; however, sample 1A has an unusual negative thermal expansion along the a axis above T_c . Of all the samples measured, sample 1A is the only sample that has $\alpha_a < 0$ for $T > T_c$. As will be discussed below, this may indicate a reduced effect of a -axis magnetic fluctuations in this sample.

Volume thermal expansion can be used to determine the pressure dependence of a second-order phase transition through the Ehrenfest relation,

$$\frac{dT_c}{dp} = \frac{\Delta\beta V_m}{\Delta C_p / T_c}. \quad (1)$$

Here, p is pressure, $\Delta\beta$ is the jump in volume thermal expansion at the phase transition, and ΔC_p is the jump in heat capacity. Because ΔC_p is always positive, the sign of the pressure dependence is determined by the sign of the jump in volume thermal expansion. Due to slight temperature offsets when measuring thermal expansion along different axes, volume thermal expansion jumps were calculated by summing the linear thermal expansion jumps at each phase transition rather than from the volume data. The results are tabulated in Supplemental Table S1 [23]. Using this relation, sample 5 is expected to have a pressure dependence of approximately $\frac{dT_c}{dp} = -0.49(04)$ K/GPa. This suppression rate agrees well with the pressure dependence of T_c determined from pressure-dependent ac calorimetry measurements (approximately -0.5 K/GPa for $P < 0.3$ GPa). In contrast, the Ehrenfest relation underestimates the pressure dependence of T_c due to the unusual a -axis behavior of sample 1A [$-0.10(04)$ K/GPa].

Now we turn to the double transition in sample 2A. Using the data from Fig. 1, Ehrenfest predicts opposite pressure dependence for the two transitions. The lower transition has $\frac{dT_{c1}}{dp} = +0.70(07)$ K/GPa and the higher transition has $\frac{dT_{c2}}{dp} = -0.65(27)$ K/GPa. This pressure dependence is most likely incorrect. It was recently shown that for samples with two transitions at ambient pressure, the transitions actually have an identical pressure dependence (see the erratum to Ref. [14]). The reason for this inconsistency is that the quasiadiabatic heat capacity measurement probes the entire volume of the sample, but the thermal expansion fixture used here will only probe a local volume of the sample when the sample is measured along its thinnest axis. For sample 2A, the c axis has a

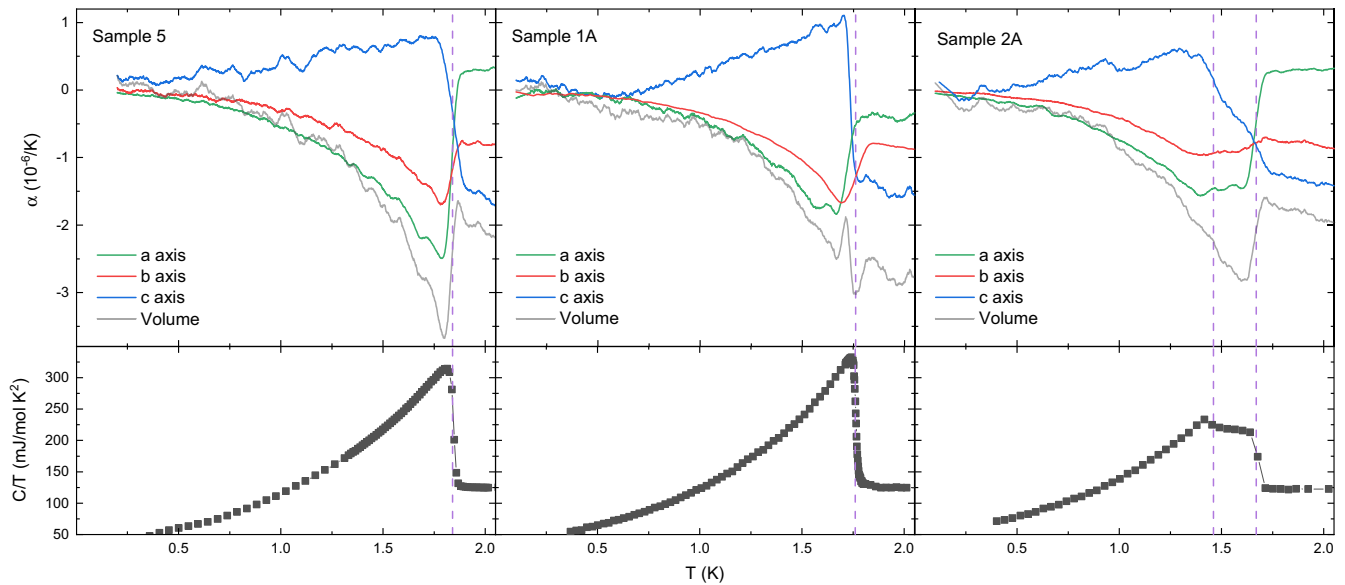


FIG. 1. Low-temperature thermal expansion (top row) and heat capacity (bottom row) of samples from different growths of UTe_2 . The purple dashed lines show the transition temperatures determined from heat capacity measurements and their relation to the thermal expansion data.

thickness of 300–360 μm compared to 2635 and 680 μm for the a and b axes, respectively.

To further unveil this issue, Fig. 2(a) shows the c -axis thermal expansion measured on multiple spots of sample 2A. Spot 1 is the same location that was measured in Fig. 1. Compared to spot 1, spot 2 has a larger contribution from the higher-temperature transition and a much smaller contribution from the lower-temperature transition. Spot 3 has the opposite weighting between the two transitions. As a result, the pressure dependence determined from Ehrenfest completely changes based on which location on the sample is used to perform the calculation. Spot 2 is the only location that predicts a negative pressure dependence for both transitions, in agreement with pressure-dependent ac calorimetry data [14].

The inhomogeneity of the double transition feature is further demonstrated by the heat capacity measurements shown in Fig. 2(b). Here, a sample showing two transitions was cut into four quadrants. The heat capacity of each quadrant was then measured individually. Remarkably, at temperatures outside the transition region, all four pieces have the same heat capacity. Near the transition, however, there is a clear difference in the weighting between the two transitions. Of the four regions, R3 has the largest percentage of the volume containing the lower-temperature transition.

The reason for the presence of exactly two transitions remains unknown, but our results indicate that the double transition feature at ambient pressure stems from sample inhomogeneity. Under pressure, however, the two transitions that appear for pressures above 0.3 GPa are an intrinsic feature of UTe_2 observed in all samples measured by multiple groups [10–14]. To confirm this, we performed pressure-dependent ac calorimetry measurements on a sample showing only a single transition at ambient pressure (sample 1B). The individual heat capacity curves from these measurements are shown in Fig. 2(c), and the pressure-temperature phase diagram is summarized in the inset. Similar to all other samples

measured under pressure, sample 1B shows clear evidence for two superconducting transitions as pressure is increased beyond 0.3 GPa. We note that a pressure-temperature phase diagram in which three second-order phase transition lines meet at a single point is not thermodynamically allowed except in very unique circumstances [10,24], and the dashed line in the inset of Fig. 2(c) is meant to represent this missing transition. Such a tetracritical point has been extensively investigated in UPt_3 [25].

Remarkably, although samples may have different T_c at ambient pressure, all samples follow the exact same pressure-temperature phase diagram, as shown in Fig. 2(d). This unified diagram is obtained by simply shifting T_c vertically to match a common value at zero pressure (i.e., $T_c = 1.8$ K). This suggests that the main effect of disorder is to suppress T_c and cause a split transition in some samples. This also reinforces that the splitting of the transition at 0.3 GPa is an intrinsic feature as it is observed in all samples measured to date. Plotting the transition temperatures in this way also shows that there is a subtle inflection in the pressure dependence of T_{c2} at 0.3 GPa (see Supplemental Sec. E [23]).

Thermal expansion to higher temperatures can provide information about the relevant energy scales in the system. Figure 3 shows the linear thermal expansion for sample 2A measured up to 200 K. At high temperatures, the thermal expansion is typically dominated by phonons. Because the nonmagnetic analog ThTe_2 has been reported to have a different crystal structure from UTe_2 [26], it is not possible to subtract an independently determined phonon background. Nonetheless, all three thermal expansion contributions become negative below 30 K, indicating a regime wherein the phonon contribution is no longer relevant. Negative thermal expansion is typically attributed to the Kondo effect, and this temperature is consistent with the Kondo temperature (20–26 K) extracted from scanning tunneling spectroscopy measurements [4]. Expansion along the a axis shows a third

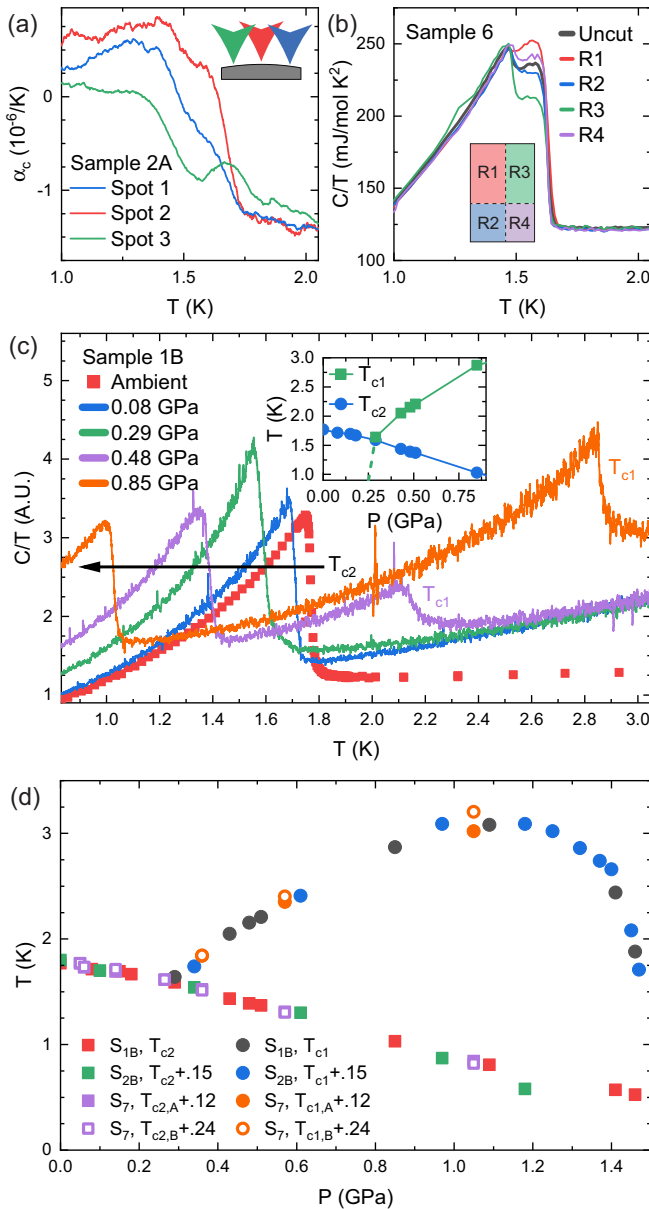


FIG. 2. (a) c -axis thermal expansion of sample 2A measured at different locations on the sample. The inset indicates the approximate positions. (b) Heat capacity of sample 6 before and after cutting into four quadrants. (c) ac calorimetry measurements of sample 1B. The inset shows a low-pressure phase diagram. (d) Pressure-temperature phase diagram of all measured samples with T_c 's adjusted to match at ambient pressure. Samples 2B and 7 were first reported in Ref. [14]. Sample 7 has two transitions at ambient pressure (A and B), both of which are tracked as a function of pressure.

energy scale, switching again from negative to positive at 11 K. This is likely due to the presence of strong magnetic fluctuations along the a axis, in agreement with previous reports [1,3,18]. While samples 2–5 all exhibit positive thermal expansion along the a axis just above the highest-temperature superconducting transition, sample 1A has negative thermal expansion along a . This may point to a difference in the strength or type of magnetic fluctuations along the a axis that is also influenced by differences in growth conditions. This

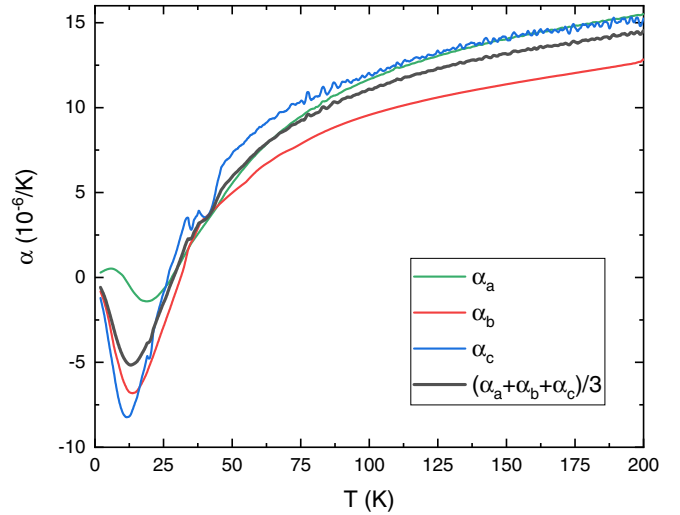


FIG. 3. Linear thermal expansion coefficients of sample 2A from 2 K up to 200 K. The gray curve shows the volume thermal expansion coefficient divided by three to better fit the scale of linear thermal expansion. The features observed near 40 K are due to gas absorption in the insulating washers that are part of the dilatometer cell.

difference is not due to sample misalignment, which would have required an alignment error of at least 26° .

Figure 4 shows the longitudinal and transverse magnetostriction measured at 2 K on sample 3 along the principal crystallographic directions. Note that the response for fields parallel to the a axis is an order of magnitude larger than along the other axes. This means that even a small field component parallel to the a axis will significantly affect measurements when applying a field along other directions. For longitudinal measurements, the sample was aligned to less than 1° using Laue diffraction. For transverse measurements, the rotation of the sample in the dilatometer cell was performed manually so the alignment errors may be up to 5° and introduce an error in measurements for fields perpendicular to the a axis.

Volume magnetostriction can be used to determine the pressure dependence of the magnetic susceptibility via Maxwell's relation [27]

$$\left(\frac{\partial \chi}{\partial P}\right)_{H,T} \propto -\left(\frac{\partial V}{\partial H}\right)_{P,T}. \quad (2)$$

At ambient pressure, the a axis is the easy magnetic axis and the b axis is the hard magnetic axis [1]. Importantly, the volume magnetostriction for fields parallel to the a axis indicates a relatively large negative pressure dependence of the a -axis susceptibility. This is consistent with a recent tight-binding model for UTe_2 , which found a large initial decrease in susceptibility along the a axis coupled with a change in the fluctuations from ferromagnetic to antiferromagnetic [28]. Further, the volume increase for fields along the c axis taken with the decrease for fields along the b axis suggests the possibility that the hard magnetic axis changes from the b axis to c axis. This has previously been claimed based on the fact that H_{c2} becomes largest along the c axis near 1.5 GPa [12]. More recently, it was experimentally confirmed via susceptibility measurements under pressure [15]. The magnetic interactions at high pressure are quite different from those at low pressure,

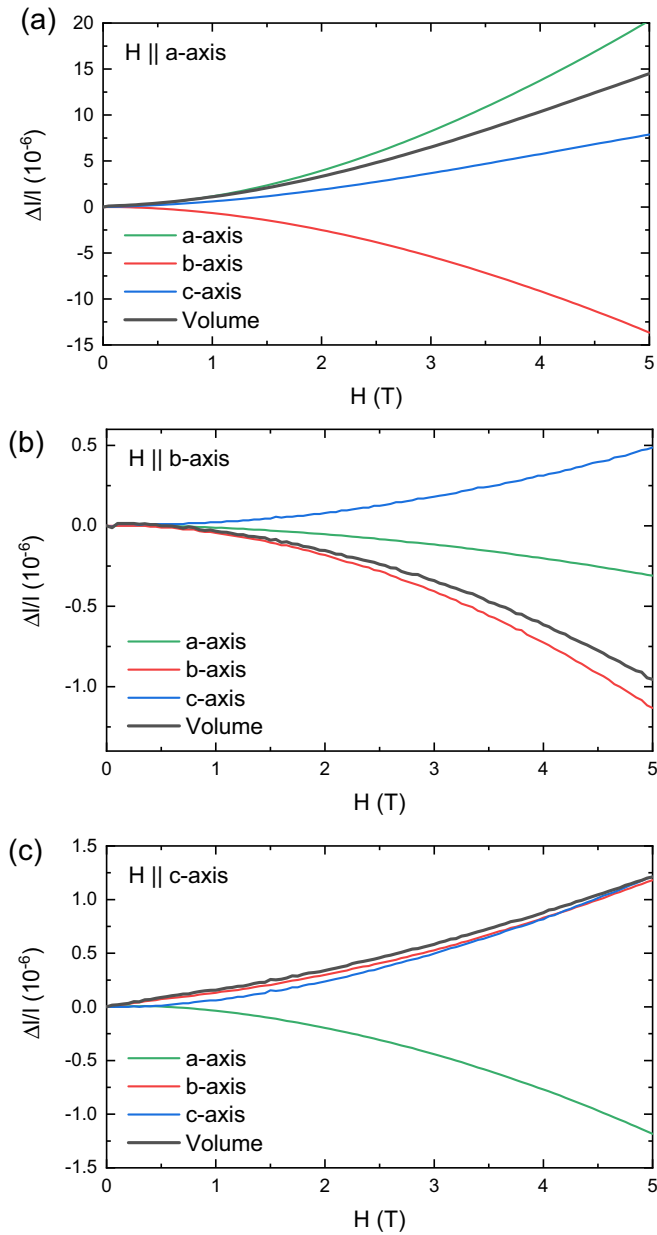


FIG. 4. Linear and volume magnetostriction for magnetic fields applied along the three principal axes of sample 3. All data were obtained at 2.0 K.

which explains the emergence of two magnetic transitions and antiferromagnetic order. In fact, the b axis becomes the easy axis in the magnetically ordered state [15]. We also highlight the possibility that samples from different batches may exhibit different magnetic properties even at ambient pressure. This

follows from the fact that sample 1A has a different sign of α_a just above T_{c2} compared to samples 2–4, as noted above. Thus, it is critical to fully characterize each single crystal of UTe_2 .

III. CONCLUSIONS

In conclusion, the combination of thermal expansion and heat capacity shows evidence for two superconducting transitions at ambient pressure only in some UTe_2 samples. Our results indicate that the double transition is due to different T_c 's in spatially separated volumes of the sample that are inhomogeneously distributed. This in turn implies that these two transitions do not arise from a multicomponent order parameter. If UTe_2 possesses a multicomponent order parameter at ambient pressure, it must be detected through other means, as evidence for two transitions in thermodynamic data is misleading in this material. Nonetheless, all samples measured to date show clear evidence for a splitting of T_c under pressure, which strongly suggests that this feature is intrinsic. Our magnetostriction data also agree with recent theoretical and experimental work that argues for a change in the nature of the magnetic interactions under pressure. Our results reveal that subtleties in sample growth play a large role in both superconductivity and magnetic fluctuations in UTe_2 . Detecting the lower-temperature transition for pressures below 0.3 GPa will play a major role in illuminating the nature of the superconducting state at ambient pressure. The origin of the sample dependence in UTe_2 may be related to structural changes, strain, or stoichiometry variations, and this topic also needs to be further investigated in the near future.

ACKNOWLEDGMENTS

We would like to thank N. Harrison, M. Jaime, and R. M. Fernandes for useful discussions as well as L. Gonzales for assistance running the experiments. Thermal expansion and magnetostriction measurements were supported by the U.S. Department of Energy, Office of Basic Energy Sciences, Division of Materials Science and Engineering project “Quantum Fluctuations in Narrow-Band Systems.” Sample synthesis at Los Alamos was performed with support from the U.S. Department of Energy, Office of Science, National Quantum Information Science Research Centers, Quantum Science Center. Pressure-dependent measurements were supported by the Laboratory Directed Research and Development program 20210064DR. C.S. and A.H. acknowledge support from UK-EPSC Grants No. EP/L015110/1 and No. EP/P013686/1. F.B.S. was supported by FAPESP under Grants No. 2016/11565-7 and No. 2018/20546-1.

- [1] S. Ran, C. Eckberg, Q.-P. Ding, Y. Furukawa, T. Metz, S. R. Saha, I.-L. Liu, M. Zic, H. Kim, J. Paglione, and N. P. Butch, *Science* **365**, 684 (2019).
 [2] D. Aoki, A. Nakamura, F. Honda, D. Li, Y. Homma, Y. Shimizu, Y. J. Sato, G. Knebel, J.-P. Brison, A. Pourret, D. Braithwaite,

G. Lapertot, Q. Niu, M. Vališka, H. Harima, and J. Flouquet, *J. Phys. Soc. Jpn.* **88**, 043702 (2019).

- [3] S. Sundar, S. Gheidi, K. Akintola, A. M. Cote, S. R. Dunsiger, S. Ran, N. P. Butch, S. R. Saha, J. Paglione, and J. E. Sonier, *Phys. Rev. B* **100**, 140502(R) (2019).

- [4] L. Jiao, S. Howard, S. Ran, Z. Wang, J. O. Rodriguez, M. Sigrist, Z. Wang, N. P. Butch, and V. Madhavan, *Nature (London)* **579**, 523 (2020).
- [5] I. M. Hayes, D. S. Wei, T. Metz, J. Zhang, Y. S. Eo, S. Ran, S. R. Saha, J. Collini, N. P. Butch, D. F. Agterberg, A. Kapitulnik, and J. Paglione, *Science* **373**, 797 (2021).
- [6] K. Ishihara, M. Roppongi, M. Kobayashi, Y. Mizukami, H. Sakai, Y. Haga, K. Hashimoto, and T. Shibauchi, [arXiv:2105.13721](https://arxiv.org/abs/2105.13721).
- [7] S. Ran, I.-L. Liu, Y. S. Eo, D. J. Campbell, P. M. Neves, W. T. Fuhrman, S. R. Saha, C. Eckberg, H. Kim, D. Graf, F. Balakirev, J. Singleton, J. Paglione, and N. P. Butch, *Nat. Phys.* **15**, 1250 (2019).
- [8] G. Knebel, W. Knafo, A. Pourret, Q. Niu, M. Vališka, D. Braithwaite, G. Lapertot, M. Nardone, A. Zitouni, S. Mishra, I. Sheikin, G. Seyfarth, J.-P. Brison, D. Aoki, and J. Flouquet, *J. Phys. Soc. Jpn.* **88**, 063707 (2019).
- [9] W. Knafo, M. Nardone, M. Valiska, A. Zitouni, G. Lapertot, D. Aoki, G. Knebel, and D. Braithwaite, *Commun. Phys.* **4**, 40 (2021).
- [10] D. Braithwaite, M. Vališka, G. Knebel, G. Lapertot, J.-P. Brison, A. Pourret, M. E. Zhitomirsky, J. Flouquet, F. Honda, and D. Aoki, *Commun. Phys.* **2**, 147 (2019).
- [11] S. Ran, H. Kim, I.-L. Liu, S. R. Saha, I. Hayes, T. Metz, Y. S. Eo, J. Paglione, and N. P. Butch, *Phys. Rev. B* **101**, 140503(R) (2020).
- [12] G. Knebel, M. Kimata, M. Vališka, F. Honda, D. Li, D. Braithwaite, G. Lapertot, W. Knafo, A. Pourret, Y. J. Sato, Y. Shimizu, T. Kihara, J.-P. Brison, J. Flouquet, and D. Aoki, *J. Phys. Soc. Jpn.* **89**, 053707 (2020).
- [13] D. Aoki, F. Honda, G. Knebel, D. Braithwaite, A. Nakamura, D. Li, Y. Homma, Y. Shimizu, Y. J. Sato, J.-P. Brison, and J. Flouquet, *J. Phys. Soc. Jpn.* **89**, 053705 (2020).
- [14] S. M. Thomas, F. B. Santos, M. H. Christensen, T. Asaba, F. Ronning, J. D. Thompson, E. D. Bauer, R. M. Fernandes, G. Fabbris, and P. F. S. Rosa, *Sci. Adv.* **6**, eabc8709 (2020).
- [15] D. Li, A. Nakamura, F. Honda, Y. J. Sato, Y. Homma, Y. Shimizu, J. Ishizuka, Y. Yanase, G. Knebel, J. Flouquet, and D. Aoki, *J. Phys. Soc. Jpn.* **90**, 073703 (2021).
- [16] C. Duan, K. Sasmal, M. B. Maple, A. Podlesnyak, J.-X. Zhu, Q. Si, and P. Dai, *Phys. Rev. Lett.* **125**, 237003 (2020).
- [17] W. Knafo, G. Knebel, P. Steffens, K. Kaneko, A. Rosuel, J. P. Brison, J. Flouquet, D. Aoki, G. Lapertot, and S. Raymond, *Phys. Rev. B* **104**, L100409 (2021).
- [18] Y. Tokunaga, H. Sakai, S. Kambe, T. Hattori, N. Higa, G. Nakamine, S. Kitagawa, K. Ishida, A. Nakamura, Y. Shimizu, Y. Homma, D. X. Li, F. Honda, and D. Aoki, *J. Phys. Soc. Jpn.* **88**, 073701 (2019).
- [19] C. Duan, R. E. Baumbach, A. Podlesnyak, Y. Deng, C. Moir, A. J. Breindel, M. B. Maple, and P. Dai, [arXiv:2106.14424](https://arxiv.org/abs/2106.14424).
- [20] L. P. Cairns, C. R. Stevens, C. D. O'Neill, and A. Huxley, *J. Phys.: Condens. Matter* **32**, 415602 (2020).
- [21] G. M. Schmiedeshoff, A. W. Lounsbury, D. J. Luna, S. J. Tracy, A. J. Schramm, S. W. Tozer, V. F. Correa, S. T. Hannahs, T. P. Murphy, E. C. Palm, A. H. Lacerda, S. L. Bud'Ko, P. C. Canfield, J. L. Smith, J. C. Lashley, and J. C. Cooley, *Rev. Sci. Instrum.* **77**, 123907 (2006).
- [22] P. F. Sullivan and G. Seidel, *Phys. Rev.* **173**, 679 (1968).
- [23] See Supplemental Material at <http://link.aps.org/supplemental/10.1103/PhysRevB.104.224501> for additional data, measurements, and procedures on thermal expansion and heat capacity, and notes on the pressure-temperature phase diagram.
- [24] S. K. Yip, T. Li, and P. Kumar, *Phys. Rev. B* **43**, 2742 (1991).
- [25] J. Sauls, *Adv. Phys.* **43**, 113 (1994).
- [26] L. A. Koscielski, E. Ringe, R. P. Van Duyne, D. E. Ellis, and J. A. Ibers, *Inorg. Chem.* **51**, 8112 (2012).
- [27] E. Fawcett, *Phys. Rev. B* **2**, 1604 (1970).
- [28] J. Ishizuka and Y. Yanase, *Phys. Rev. B* **103**, 094504 (2021).